Supplementary Information: Generation and propagation of flexoelectricity-induced solitons in nematic liquid crystals

Xingzhou Tang,[†,‡] Noe Atzin,[†] Ali Mozaffari,[†,¶] Soumik Das,[§,‖] Nicholas L. Abbott,[§] and Juan J. de Pablo[*,†,⊥]

†*Pritzker School of Molecular Engineering, The University of Chicago, Chicago, Illinois 60637, U.S.A.*

‡*College of Flexible Electronics (Future Technology), Nanjing University of Posts and Telecommunications, Nanjing 210023, China*

¶*OpenEye Scientific, Cadence Molecular Sciences, Boston, Massachusetts 02114, U.S.A*

§*Smith School of Chemical and Biomolecular Engineering, Cornell University, Ithaca, New York 14853, U.S.A.*

‖*Department of Chemical Engineering, Indian Institute of Technology Kanpur, Kanpur, 208016, India*

⊥*Center for Molecular Engineering, Argonne National Laboratory, Lemont, Illinois 60439, U.S.A.*

E-mail: depablo@uchicago.edu

Supplementary Information

Theoretical framework details

elastic free energy

The elastic free energy density can be described by the Frank-Oseen free energy,[1–3] where the nematic order parameter is assumed to be uniform. The value of Ls in the simulation is taken by studying the relationship between elastic constants (L_i) and Frank constants (K_{ij}). The Frank-Oseen free energy can be represented as follows:

$$f_{\text{elas}} = \frac{1}{2}\left(K_{11}-K_{24}\right)\left(q_{il}\partial_j q_{jl}\right)^2 + \frac{1}{2}\left(K_{22}-K_{24}\right)\left(\epsilon_{ijk}q_{il}\partial_j q_{kl}\right)^2 + \frac{1}{2}K_{33}\left(q_{il}\partial_i q_{kl}\right)^2 + \frac{1}{2}K_{24}Tr\left(\mathbf{\Delta}^2\right). \tag{S1}$$

where $q_{ij} = n_j n_j = \frac{1}{3}(\delta_{ij}+2Q_{ij}/s)$ and the four terms are splay, twist, bend, and saddle-splay respectively. Because $\boldsymbol{n}$ is a unit vector, we have:

$$n_i\partial_j n_k = q_{il}\partial_j q_{kl}. \tag{S2}$$

By making appropriate contractions of that equation, we can derive the bend vector

$$B_k = -n_j\partial_i n_k = -q_{il}\partial_j q_{kl}, \tag{S3}$$

and the twist pseudoscalar

$$T = \epsilon_{ijk}n_i\partial_j n_k = \epsilon_{ijk}q_{il}\partial_j q_{kl}. \tag{S4}$$

We define a splay vector $\boldsymbol{S} = S\boldsymbol{n}$ which is even in $\boldsymbol{n}$ so that we can describe the splay in terms of q_{ij}.

$$S_i = Sn_i = n_i \partial_j n_j = q_{il} \partial_j q_{jl}. \tag{S5}$$

$\boldsymbol{\Delta}$ in the saddle-splay term is "biaxial splay". It is a traceless symmetric tensor in the plane perpendicular to $\boldsymbol{n}$. It has two degrees of freedom as a traceless symmetric tensor in a plane. It can be defined as the third-rank tensor

$$\begin{aligned} \Delta_{ij} n_k &= \frac{1}{2} \left[n_k \partial_i n_j + n_k \partial_j n_i + n_k n_i B_j + n_k n_j B_i - S n_k (\delta_{ij} - n_i n_j) \right] \\ &= \frac{1}{2} \left[q_{kl} \partial_i q_{jl} + q_{kl} \partial_j q_{il} + q_{ki} B_j + q_{kj} B_i - S_k (\delta_{ij} - q_{ij}) \right]. \end{aligned} \tag{S6}$$

By neglecting the K_{24} term, the free energy density is simplified as

$$f_{\text{elas}} = \frac{1}{2} K_{11} \left(q_{il} \partial_j q_{jl} \right)^2 + \frac{1}{2} K_{22} \left(\epsilon_{ijk} q_{il} \partial_j q_{kl} \right)^2 + \frac{1}{2} K_{33} \left(q_{il} \partial_i q_{kl} \right)^2. \tag{S7}$$

The relationship between elastic constants (L_i) and Frank constants (K_{ij}) is given by:[4]

$$\begin{aligned} L_1 &= \frac{2}{27 s^2} (K_{33} - K_{11} + 3K_{22}), \\ L_2 &= \frac{2}{9 s^2} K_{11}, \\ L_3 &= -\frac{2}{9 s^2} K_{22}, \\ L_6 &= \frac{4}{27 s^2} (K_{33} - K_{11}). \end{aligned} \tag{S8}$$

The energy well depth f_{LdG} (3) provides a measure of the threshold value for f_{elas} (4) at which distortions become so energetically costly that local melting of the nematic order occurs. This length $l = \xi_N$, the nematic correlation length (or coherence length), sets the size of the defect core:

$$\xi_N = \sqrt{L_1 / |f_{\text{LdG}}|}. \tag{S9}$$

flexoelectric free energy

The flexoelectric density energy is described from the coupling between the nematic distortion and electric polarization, and the polarization field in the uniaxial framework, P_i, is[5–7]

$$\begin{aligned} P_{\mathrm{i}} &= \frac{1}{2}(e_{11}+e_{33})s\partial_j(n_i n_j)+\frac{1}{2}(e_{11}-e_{33})s(n_i\partial_j n_j - n_j\partial_j n_i) \\ &+ r_1\partial_i s + r_2(2n_i n_j-\delta_{ij})\partial_j s. \end{aligned} \tag{S10}$$

e_{11} and e_{33} are the usual flexoelectric terms, corresponding to splay and bend. r_1 and r_2 are the order polarization. The r_1 term couples to the gradient of nematic order parameter s, describing a polarization across the interface independent of the alignment. The r_2 term is alignment dependent, and the homeotropic configuration and planar configuration have opposite polarities.

Substitution of equation 1 into 10 and comparison with S10, the relationship among e_{11}, e_{33}, r_1, r_2 and χs yields

$$\begin{aligned} e_{11} &= 2\chi_0 + s\chi_+ + s\chi_- \\ e_{33} &= 2\chi_0 + s\chi_+ - s\chi_- \\ r_1 &= \frac{1}{3}\chi_0 + \frac{5}{3}s\chi_+ + s\chi_2 \\ r_2 &= \chi_0 + s\chi_+. \end{aligned} \tag{S11}$$

In cases where the order parameter s is uniform, it is feasible to neglect the order polarization, as well as the χ_2 term. However, in our study, since s is not uniform, we do not disregard these terms. This consideration ensures the accuracy and relevance of our analysis, particularly in scenarios where the variation in the order parameter significantly influences the system's behavior.

Transition Process of the director field in DC electric field

We explore the influence of the electric field direction and surface patches on the relaxation of the director field under a DC field, demonstrating the transition from a uniform state.

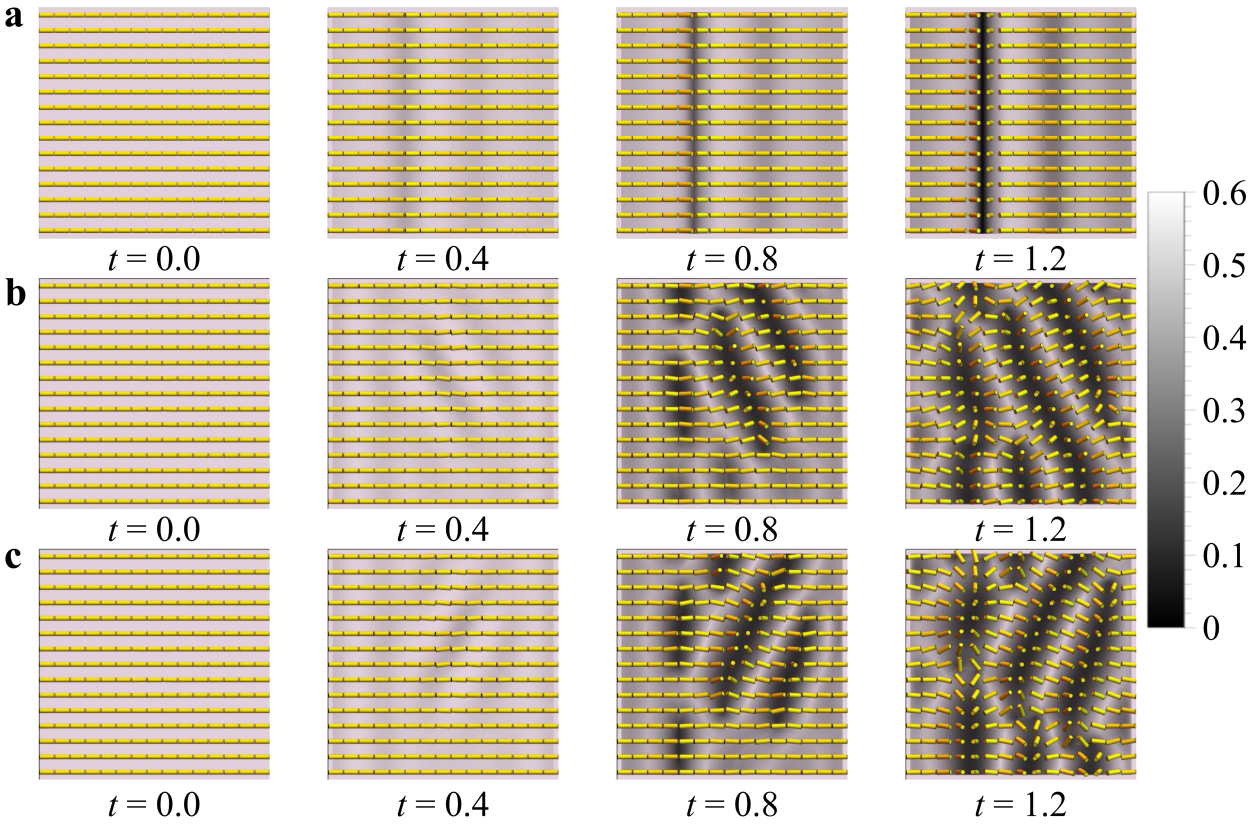

Figure S1: Transition process of the director field at the plane of $z = 0$, illustrating changes in the order parameter. (a) Initially, the system is uniform; (b) A surface patch is introduced at $z = z_{max}$ with the electric field directed along $+z$; (c) A similar surface patch as in (b) is applied, but with the electric field directed along $-z$.

Figure S1 illustrates the transition process, correlating with **Figure** 1. In **Figure** S1 (a), the director field partially rotates towards the z-axis. An expanding defect ring is observed, which stabilizes at a position very close to the top and bottom surfaces. In **Figure** S1 (b) and (c), a surface patch, as depicted in **Figure** 1 (b), is introduced. This addition leads to the gradual formation of stripes, with their alignment being influenced by the direction of the electric field.

Effect of the Electric Field's Nonlocality

In this section, we delve into the incorporation of Maxwell's equations into our simulations. We define the current density, j_i, following the formulation provided by Landau et al.:[8]

$$j_i = \sigma(E_i + \epsilon_{ikn}\frac{v_k}{c}B_n). \tag{S12}$$

Here, σ represents the electric conductivity. Considering the second term, which is related to the magnetic field, the velocity of the nematic molecules (v_k) is considerably lower than the speed of light (c), leading us to disregard the magnetic field's contribution in this analysis.

Further, we utilize Maxwell's equations to describe the electric field ($\boldsymbol{E}$) as follows:

$$\begin{aligned} -\epsilon_0(\bar{\epsilon}\partial_i E_i + \epsilon_a Q_{ij}\partial_i E_j) = &-\epsilon_0\epsilon_a E_j\partial_i Q_{ij} + \frac{4}{3}\chi_0\partial_{ij}Q_{ij} + \frac{4}{3}\chi_+\partial_{ij}(Q_{ik}Q_{kj}) \\ &+ \frac{1}{3}\chi_2\partial_{ii}(Q_{jk}Q_{kj}) + \frac{4}{9}\chi_-(\partial_i Q_{ik}\partial_j Q_{kj} - \partial_i Q_{jk}\partial_j Q_{ij}). \end{aligned} \tag{S13}$$

Solving equation S13 necessitates iterative calculations across the simulation grid at each time step. Introduction of flexoelectric effects leads to deviations in the directors' orientation from their initial alignment, causing gradients within the director field to vary. These alterations in gradient levels contribute to the nonlocal behavior of the electric field. In scenarios where the applied voltage is high, the director field undergoes modifications across various locations, resulting in the generation of solitons throughout the system. Conversely, at lower voltages where soliton emission is limited to areas of irregularity, the impact of this effect can be considered negligible.

SFG by a Gold Surface with Tilt

If there is a small average tilt angle θ with the gold grains concerning the boundary normal, then it can be shown that for p-polarized IR and visible beams, the p-polarized

sum-frequency electric field (i.e., PPP configuration) is approximately equal to

$$\begin{aligned} E_p &\approx \alpha_{iso} - \theta cos(\Phi) + \theta\gamma_{anis} cos(2\Phi) + \delta_{anis} cos(3\Phi) \\ &\approx A[\alpha'_{iso} - \theta\beta'_{iso} cos(\Phi) + \theta\gamma'_{anis} cos(2\Phi) + \delta'_{anis} cos(3\Phi)]. \end{aligned} \tag{S14}$$

with $\alpha_{iso} \approx L_{x1}(L_{x3}L_{z2}\chi_{xzx} + L_{x2}L_{z3}\chi_{zxx})$, $\beta_{iso} \approx L_{x3}L_{x2}L_{x1}(\chi_{xxz} + \chi_{xzx} + \chi_{zxx})$, $\gamma_{anis} \approx (L_{x3}L_{x2}L_{x1} + L_{z3}L_{x2}L_{x1} + L_{x3}L_{z2}L_{x1})\chi_{xxx}$, and $\delta_{anis} \approx L_{x3}L_{x2}L_{x1}\chi_{xxx}$, with for the visible and IR waves $L_{xi} = e_{xi}F_{xi}$, $L_{zi} = e_{zi}F_{zi}$ and for the visible beam $L_{x3} = e_{x3}F_{x3}/\beta_3$, $L_{z3} = e_{z3}F_{z3}/\beta_3$. The χs are the azimuthal tensor parameters. The normalization constant A is the amplitude factor chosen such that $\alpha_{iso} = 1$.

For a p-polarized IR beam, an s-polarized visible beam and the s-polarized sum-frequency electric field (i.e., PSS configuration) are approximately equal to

$$\begin{aligned} E_p &\approx \alpha_{iso} - \theta\beta_{iso} cos(\Phi) - \theta\gamma_{anis} cos(2\Phi) - \delta_{anis} cos(3\Phi) \\ &\approx A[\alpha'_{iso} - \theta\beta'_{iso} cos(\Phi) - \theta\gamma'_{anis} cos(2\Phi) - \delta'_{anis} cos(3\Phi)]. \end{aligned} \tag{S15}$$

with $\alpha_{iso} = L_{y3}L_{y2}L_{z1}\chi_{xxz}$, $\beta_{iso} = L_{y3}L_{y2}L_{x1}\chi_{xxz}$, $\gamma_{anis} = L_{y3}L_{y2}L_{z1}\chi_{xxx}$, and $\delta_{anis} = L_{y3}L_{y2}L_{x1}\chi_{xxx}$. The permittivity of gold is complex-valued, which makes the L factors complex and so also α_{iso}, β_{iso}, γ_{iso}, and δiso. In this paper, we assume the constants α'_{iso}, β'_{iso}, γ'_{iso}, and $\delta iso'$and are real, which is consistent with the approach followed in Everitt et al.[9]

Numerical details

While the scalar order parameter S indicates that simulation parameters are appropriate for experimental realizations, here we also show how each of these parameters can be matched to experimental values. In order to nondimensionalization, we need four characteristic parameters to represent length, time, electric charge, and mass. We take $\xi_N (= \sqrt{CL_1/B^2} \sim$

0.1), $\tau(=\Gamma_1\xi^2/L_1 \sim 10^{-3})$, χ_-, and L_1 respectively because these parameters are the dominant factors in the simulation. In order to compare with experiments, we consider the ratio of U over U_{max}, where U_{max} is the value where the system enters the chaotic regime even at low frequency, which is 87 in the simulation. Then the real data for the voltage and frequency can be calculated in the following way:

$$\begin{aligned} U_{real} &= 1.15 U_{simulation} \frac{(\Pi_U)_{simulation}}{(\Pi_U)_{real}} \\ &= 1.15 U_{simulation} \frac{5/5}{(10^{-11} C\, m^{-1})/(10 \times 10^{-12} N)} \\ &= 1.15 U_{simulation} V. \end{aligned} \tag{S16}$$

Similarly,

$$\begin{aligned} \omega_{real} &= \omega_{simulation} \frac{(\Pi_\omega)_{simulation}}{(\Pi_\omega)_{real}} \\ &= \omega_{simulation} \frac{0.001}{0.01 s} \\ &= 0.1 \omega_{simulation} Hz. \end{aligned} \tag{S17}$$

In our simulation, we set the voltage range from 0 to 85, and the frequency range from 0 to 10,000. These values are subsequently converted into normalized voltage ($\widetilde{U}$) ranging from 0 to 100V, and normalized frequency ($\widetilde{\omega}$) from 0 to 1000Hz. This approach allows us to align our simulation parameters with realistic and experimentally relevant scales, facilitating an accurate and meaningful comparison between simulation results and experimental data.

3D Structure of Soliton

In this section, we represent the structure of a soliton and show the force from the flexoelectricity.

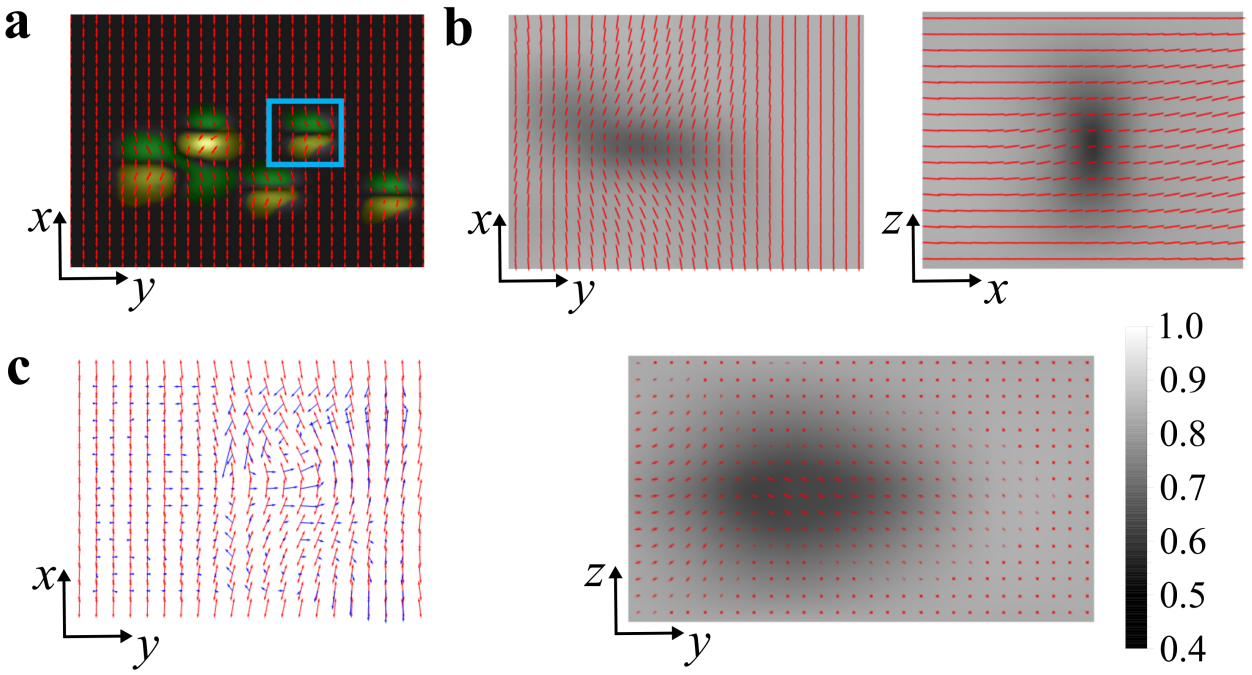

Figure S2: Topology of the bullet. A bullet is analyzed in the blue frame of (a). In (b), the structure of the bullet and figures of the nematic order parameter are shown in x-y, y-z, and x-z plane respectively. (c)shows the forces of flexoelectricity on the x-y plane for each director.

Bullet-like solitons are emitting out of the butterfly-like patch in **Figure** S2 (a), and we analyze the bullet in the blue frame. **Figure** S2 (b) shows the director field and nematic order parameter in x-y, y-z, and x-z plane respectively. The black region of the figure has a low value of S. On the x-y plane, the S is small in the region of the bullet and a ring-like structure is represented in the y-z plane. The x-z plane shows the cross-section of the ring.

We also analyze the forces from flexoelectricity in **Figure** S2 (c), which is the spatial gradient of the flexoelectric energy. In this figure, we can find the forces on the 'wings' of the bullet pointing inside. The structure of the bullet is unstable without the electric field, and under the elastic force, the bullet would shrink imminently. So the effect of flexoelectricity helps to stabilize the bullet. Also, we can find the total force pointing in the right direction, which is the direction of the soliton moving. So the flexoelectricity also drives the bullet.

References

(1) Mori, H.; Gartland, E. C.; Kelly, J. R.; Bos, P. J. Multidimensional director modeling using the Q tensor representation in a liquid crystal cell and its application to the it cell with patterned electrodes. *Japanese Journal of Applied Physics, Part 1: Regular Papers and Short Notes and Review Papers* **1999**, *38*, 135–146.

(2) Nehring, J.; Saupe, A. Calculation of the Elastic Constants of Nematic Liquid Crystals. *The Journal of Chemical Physics* **1972**, *56*, 5527–5528.

(3) Selinger, J. V. Interpretation of saddle-splay and the Oseen-Frank free energy in liquid crystals. *Liquid Crystals Reviews* **2018**, *6*, 129–142.

(4) Mori, H.; Gartland Jr, E. C.; Kelly, J. R.; Bos, P. J. Multidimensional director modeling using the Q tensor representation in a liquid crystal cell and its application to the π cell with patterned electrodes. *Japanese journal of applied physics* **1999**, *38*, 135.

(5) Barbero, G.; Dozov, I.; Palierne, J.; Durand, G. Order electricity and surface orientation in nematic liquid crystals. *Physical review letters* **1986**, *56*, 2056.

(6) Blow, M. L.; da Gama, M. T. Interfacial motion in flexo-and order-electric switching between nematic filled states. *Journal of Physics: Condensed Matter* **2013**, *25*, 245103.

(7) Alexe-Ionescu, A.-L. Flexoelectric polarization and second order elasticity for nematic liquid crystals. *Physics Letters A* **1993**, *180*, 456–460.

(8) Landau, L. D.; Bell, J. S.; Kearsley, M.; Pitaevskii, L.; Lifshitz, E.; Sykes, J. *Electrodynamics of continuous media*; elsevier, 2013; Vol. 8.

(9) Everitt, D. L.; Miller, W. J.; Abbott, N.; Zhu, X. Evolution of a preferred orientation of polycrystalline grains in obliquely deposited gold films on an amorphous substrate. *Physical Review B* **2000**, *62*, R4833.